Low-frequency transient dynamic clusters in simulated amorphous $Ni_{0.5}Zr_{0.5}$ around the glass temperature

I. Ladadwa and H. Teichler
Institut für Materialphysik and SFB 602, Universität Göttingen, 37077 Göttingen, Germany
(Received 21 December 2007; revised manuscript received 14 July 2008; published 10 October 2008)

Molecular dynamics results are reported concerning cooperatively rearranging regions in simulated $Ni_{0.5}Zr_{0.5}$ melts down to 700 K. Emphasis is laid on discriminating between clusters of mobile atoms (CMA) from low-frequency dynamics and the all-frequency case, where the former characterize fluctuations and relaxations on the scale of the late β regime and α decay, while the latter include, in addition, reversible high-frequency vibrations. Separation of the low-frequency part of the dynamics is carried out by low-pass filtering, exploiting the separation of time scales below the critical temperature T_c of the mode-coupling theory. With increasing temperature, the low-frequency and all-frequency dynamics merge in the range of T_c when the separation of time scales disappears. In the low-frequency CMA, the average size of correlated clusters of connected atoms turns out to be nearly one order of magnitude larger than in the all-frequency CMA. The low-frequency CMA appear as local clusters propagating extremely slowly in space with characteristic time scale of μs at 700 K, the scale of the onset of α decay.

DOI: 10.1103/PhysRevE.78.041503 PACS number(s): 64.70.Q−, 61.20.Ja, 61.20.Lc

I. INTRODUCTION

The glass transition, observed in various types of liquids, is one of the challenging unsolved problems in actual condensed matter physics. One of its striking characteristics is the dramatic increase of the viscosity by more than ten orders of magnitude in a rather narrow temperature range above the glass transition. Adam and Gibbs [1] promoted the idea that this increase reflects the growth of cooperatively rearranging regions (CRRs) with decreasing temperature, where the CRRs are spatial units that carry the rearrangement dynamics in the vitrifying melt. With the understanding that the CRR formation rate reduces with increasing size, the glass transition follows in this theory from a divergence of the size of the CRRs at a temperature that agrees with Kauzmann's [2] critical temperature T_K.

There exist a large number of further theoretical approaches to the glass transition, which also are based on the idea of heterogeneous dynamics in the melt, which means the existence of CRRs. Some recent ones are, for example, the theory of dynamical facilitation described by Garrahan and Chandler [3,4], the approach by Matyushov and Angell [5], or the proposal by Langer [6]. Accordingly, the search for CRRs and an analysis of their sizes is a central issue in the field of the glass transition.

At present, important information on the dynamical heterogeneity in vitrifying melts is gained from molecular dynamics (MD) simulations. In the last years, by a cluster size analysis (CSA)—for example, [7–10] and references therein—a systematic approach has been developed to estimate the mean size of correlated rearranging clusters above and around the critical temperature T_c of the mode-coupling theory [11]. Further, there are our own studies [12–15], which concentrate on the mechanisms active in heterogeneous dynamics at low temperatures in suitably relaxed structures down to T_K, and there are room-temperature studies in extreme rapidly quenched structures [16].

The present contribution reports results from combining the methods of the CSA with our findings on the mechanisms of heterogeneous dynamics in vitrifying metallic melts around T_K. In this temperature regime, the cage effect is fully active. It allows a characterization of the dynamical processes in high-viscous complex liquids as (i) vibration of atoms in the cages formed by the shell of next-neighbor particles, (ii) reversible short-time excursions over the cage barriers by individual and correlated chains of atoms, and (iii) irreversible and long-lasting reversible low-frequency rearrangements of groups of atoms [12–15]. As deduced in our MD studies on the NiZr system [12–15] and recently confirmed for the binary Lennard-Jones model [17], the low-frequency dynamics takes place in the form of bursts or avalanches [12,13], which are local events in space and time and involve extended clusters of atoms [14,15]. These events describe the probing of the potential energy landscape (PEL) in the course of α decay, while the high-frequency dynamics reflects the reversible excitations.

CSA studies have considered so far superpositions of all kinds of dynamical processes, thus mixing vibrations and low-frequency rearrangements. Here we present results from analyzing clusters formed only by atoms active in the irreversible, low-frequency dynamics. As in our recent studies for $Ni_{50}Zr_{50}$ [12–15], here we exploit the fact that below T_c, when the cage effect is active, there is a marked separation of time scales between the reversible high-frequency dynamics and the low-frequency processes in well-relaxed vitrifying structures. Accordingly, the high-frequency contributions to the dynamics can be eliminated by simple low-pass filtering [14,15]. The separation of time scales is visible, e.g., in the intermediate scattering functions or the mean-square displacements, as a flat plateau with negligible slope, extending over more than three decades in time [14]. The necessary separation of time scales takes place, however, only in suitably relaxed structures, which in our case means that the α-relaxation time by aging shifts towards the microsecond regime.

Further organization of the contribution is as follows: Section II gives a brief description of the model and meth-

ods. Section III is devoted to the presentation of the results. Section IV provides a short discussion, and Sec. V presents concluding remarks.

II. MODEL AND METHODS

A. Simulation model

The MD calculations are carried out as isothermal-isobaric (N,T,p) simulations for a binary $Ni_{50}Zr_{50}$ system with zero pressure. The equations of motion are integrated numerically by a fifth-order predictor-corrector algorithm with time step $\delta t=2.0\times10^{-15}$ s. An ensemble of $N=5184$ atoms is considered in an orthorhombic box with periodic boundary conditions and variable box lengths evaluated from the zero-pressure condition.

The simulations were performed using pair potentials adapted to the *first-principles* Hausleitner-Hafner model [18] for $Ni_{50}Zr_{50}$ and a volume-dependent electron-gas term according to Finnis [19]. The simulations cover the temperature range between 1500 and 700 K and time windows up to 2 μs. The considered temperature interval includes the critical temperature of the mode-coupling theory of the system, $T_c\approx1120$ K [20,21], as well as its Kauzmann temperature $T_K\approx750$ K [22] and the glass temperature $T_g\approx1050$ K [20,21] relevant for the applied cooling rate.

B. Low-frequency dynamics

Molecular dynamics simulations provide the individual atom motions $\vec{r}_n(t)$, which involve particle vibrations, reversible over-barrier excursions of (chains of) atoms, and long-living low-frequency or irreversible dynamical events. As discussed in [14,15], at temperatures below about 1000 K, low-pass filtering allows for the elimination of high-frequency fluctuations and a separate study of low-frequency dynamics. The latter includes from their definition the irreversible relaxation processes in the melt. Here, as in [14,15], low-pass filtering is carried out by introducing smoothed atomic paths

$$\bar{\vec{r}}_n(t)=\int_{-\infty}^{\infty}\vec{r}_n(t')\frac{e^{-(t'-t)^2/2\tau^2}}{\sqrt{2\pi\tau^2}}dt'. \quad (1)$$

In the numerical evaluation, the integration is substituted by summation over a discrete set of equidistant time points with 0.1 ns step width, where the sum is limited to $|t'-t|<5\tau$. The $\bar{\vec{r}}_n(t)$ obviously depend on the smoothing time τ. In our previous studies, $\tau=3$ ns turned out as an appropriate choice. We here shall use τ values of this order of magnitude and compare the predictions from these low-frequency (LF) dynamics with the unfiltered all-frequency (AF) results.

C. Mobility and clusters of most mobile atoms

1. All-frequency and low-frequency mobility of atoms

In order to compare the heterogeneity of LF dynamics with the AF behavior, we adopt the procedure of Donati *et al.* [7] and measure the mobility of particle n in the time interval $[t,t+\Delta t]$ by the quantity

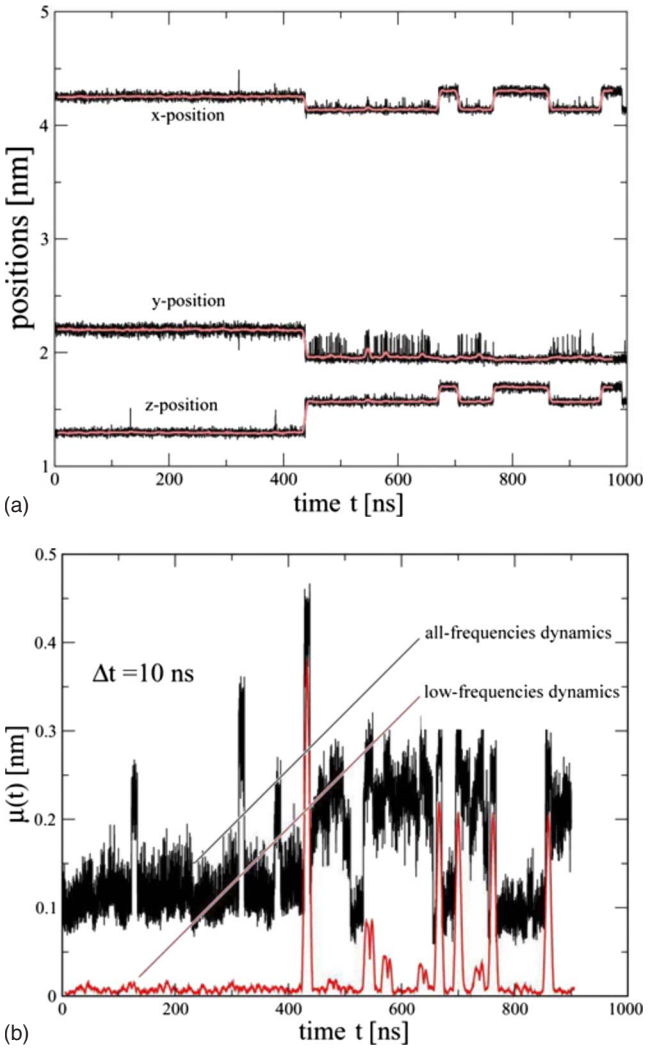

FIG. 1. (Color online) (a) Native (black lines) and smoothed low-pass-filtered coordinates (light, red lines) of arbitrary particle n as function of time. (b) Mobility parameter attributed to particle n from native coordinates (noisy, black lines) and from low-pass-filtered dynamics (lower red line). The mobility is determined for a time interval $\Delta t=10$ ns. Low-pass filtering is carried out with $\tau=3$ ns.

$$\mu_n(t,\Delta t)=\max\{|\bar{\vec{r}}_n(t')-\bar{\vec{r}}_n(t)|\}_{t'\in[t,t+\Delta t]}, \quad (2)$$

which is the maximum displacement of atom n within the time interval $[t,t+\Delta t]$. Unlike previous CSA studies (e.g., [7–10,23–26]), here we use AF or LF coordinates $r_n(t)$ in order to analyze both AF and LF atomic mobility.

The definition, Eq. (2), allows ascribing to each atom a quantitative value of mobility as a continuous function of time t, interval length Δt, and smoothing time τ. Figure 1 demonstrates the effects of Eqs. (1) and (2): The upper panel shows the trajectories $x_n(t)$ and $\bar{x}_n(t)$ of one particular atom. While the original trajectories involve all vibrations and fluctuations, the low-pass-filtered, smoothed ones present the long-time dynamics only. The lower panel of Fig. 1 displays, as an example, the mobility of the chosen atom as a function of time t and arbitrarily selected interval length $\Delta t=100$ ns

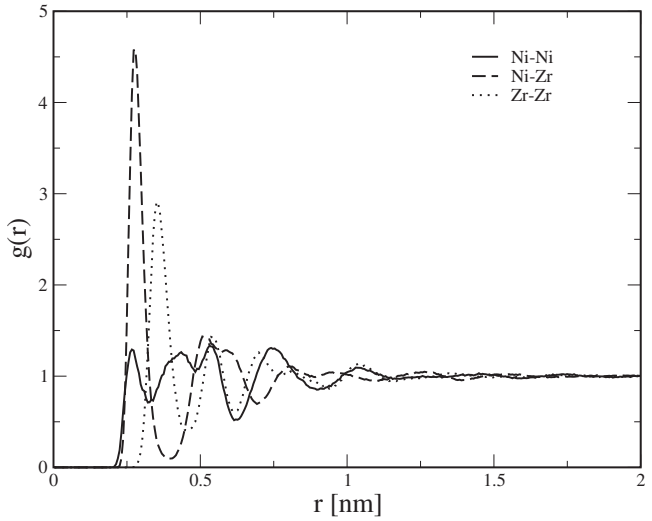

FIG. 2. Partial radial distribution functions for Ni-Ni, Ni-Zr, and Zr-Zr pairs in simulated $Ni_{0.5}Zr_{0.5}$ at 700 K.

from LF dynamics with $\tau=3$ ns and from AF dynamics with $\tau=0$. In the mobility, the main effect of LF filtering is visible for times t below 0.4 μs. In this time range, the atom carries out short-time excursions of about 0.25 nm in space, detectable in the upper panel of Fig. 1 in the original positions of the atom as short, vertical lines. As displayed in the lower panel, these excursions induce large values of AF mobility over the full interval length of 100 ns, although the excursions have lifetimes below 1 ns. Low-pass filtering averages out these excursions and, as obvious from Fig. 1, they do not contribute to the LF mobility.

2. Clusters of most mobile atoms

In our further analysis we also follow closely the formalism of Donati *et al.* [7] in the version used by Vogel and Glotzer [10] for SiO_2. Our treatment includes, however, two minor modifications. First, we have the smoothing time τ as an additional parameter, which characterizes the eliminated high-frequency fluctuations. Second, in our analysis we shall not discriminate between Ni and Zr atoms when evaluating the clusters of connected highly mobile atoms. The latter modification takes care of the fact that in the present system there is a strong short- and medium-range order. Ni resides in trigonal prismatic holes formed mainly by Zr atoms [18,27], which yields that the probability for Ni-Ni neighbors is markedly reduced in favor of Ni-Zr neighbors and Ni-Ni next-nearest neighbors. This medium-range order is clearly seen in the simulated radial distribution functions, Fig. 2, and as a pre-peak in neutron-scattering experiments for glass [28].

Following [7–10], we introduce for each t, Δt, and τ the set of the N_c most mobile atoms, $X(t,\Delta t,\Phi,\tau)$ [cluster of mobile atoms (CMA)], which includes the atoms with the largest mobility in the interval $[t,t+\Delta t]$ for a given τ. Here the fraction $\Phi=N_c/N$ is used as an independent parameter, with N the total number of atoms in the simulation box.

In the next step, the set $X(t,\Delta t,\Phi,\tau)$ is partitioned into connected clusters of mobile atoms (CCMA). A CCMA consists of all those particles that at time t are connected by paths of nearest-neighbor steps. Two atoms are denoted as nearest neighbors if their spatial distance is less than the minimum, $r_{\min}$, between first- and second-neighbor shells in the radial distribution function (RDF), Fig. 2. Since we have a binary system with two types of particles and nonadditivity of particle size, there are three values of the critical distance, $r_{\min}=0.34$, 0.39, and 0.46 nm for NiNi, NiZr, and ZrZr pairs, respectively.

This definition yields a unique partitioning of the set $X(t,\Delta t,\Phi,\tau)$ into CCMA, where the analysis mainly concentrates on the size of these clusters, which means the number n of atoms in each cluster.

For quantifying the cluster size distribution, the distribution function $P(n,\Delta t,\Phi,\tau)$ is introduced, which is the normalized probability of finding a cluster of size n for time interval Δt and smoothing time τ, when averaging over the initial times t:

$$\sum_n P(n,\Delta t,\Phi,\tau)=1. \tag{3}$$

The mean cluster size follows [24–26] as

$$S_N(\Delta t,\Phi,\tau)=\sum_n nP(n,\Delta t,\Phi,\tau). \tag{4}$$

In order to eliminate from the mean cluster size the contributions of clusters formed by statistical fluctuations in a random set of N_c atoms, a normalized value is deduced from $S_N(\Delta t,\Phi,\tau)$ by

$$\bar{S}_w(\Delta t,\Phi,\tau)=S_N(\Delta t,\Phi,\tau)/S_N^*, \tag{5}$$

with S_N^* the mean size of connected clusters in randomly selected sets of N_c atoms.

III. RESULTS

A. All-frequencies dynamics

Figure 3 displays the results for the normalized mean size of clusters of highly mobile atoms, $\bar{S}_w(\Delta t)$, obtained for simulated $Ni_{0.5}Zr_{0.5}$ without low-pass filtering for $\Phi=0.07$ and time intervals Δt up to 1 μs at temperatures between 1500 and 700 K. As already mentioned, this temperature range covers the critical temperature of the mode coupling theory of our system, $T_c\approx 1120$ K [20,21], as well as its Kauzmann temperature $T_K\approx 750$ K [22] and the glass temperature $T_g\approx 1050$ K [20] relevant for the applied cooling rate.

The present data have to be compared to those provided in the literature for glassy SiO_2 [7,26], the Lennard-Jones system [7,10], or the Dzugutov model [9,25]. The main difference to the so-far published data comes from the fact that we include the temperature range below T_c and T_K. This makes it necessary to consider much longer intervals Δt. Down to temperatures of 810 K, there is overall agreement between the present observations and the so-far published results: The mean cluster size increases with decreasing temperature. A particular feature is found in our data when going from

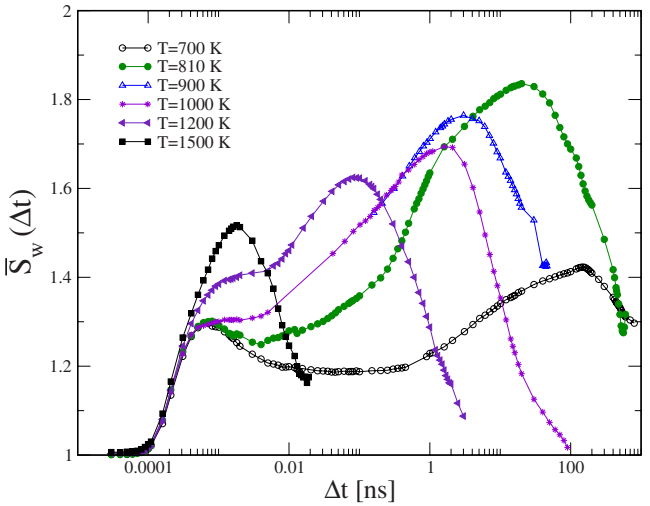

FIG. 3. (Color online) Normalized mean size of connected clusters of mobile atoms from all-frequency dynamics in simulated $Ni_{0.5}Zr_{0.5}$ as function of interval length Δt for fraction value $\Phi = 0.07$ at various temperatures.

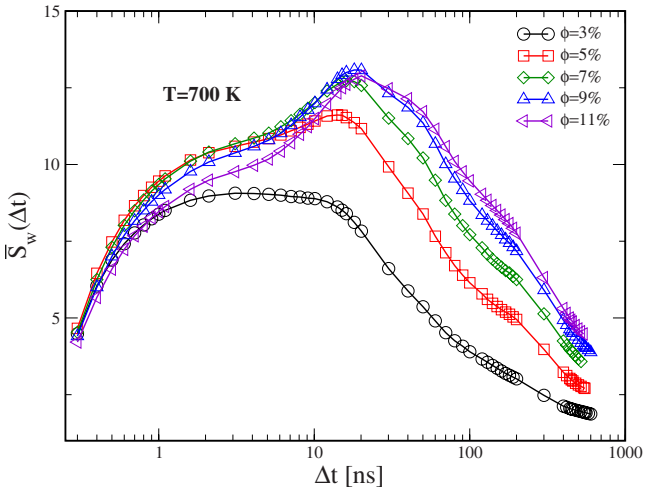

FIG. 5. (Color online) Normalized mean size of connected clusters of mobile atoms from low-frequency dynamics ($\tau = 3$ ns) in simulated $Ni_{0.5}Zr_{0.5}$ as a function of interval length Δt at $T = 700$ K for a fraction value Φ between 0.03 and 0.11.

810 to 700 K. In this regime, around the Kauzmann temperature T_K, the cluster size decreases with decreasing temperature.

B. Cluster size of mobile atoms from low-pass-filtered dynamics

In order to demonstrate the separation of time scales between high- and low-frequency dynamics in our $Ni_{0.5}Zr_{0.5}$ model, Fig. 4 presents incoherent intermediate scattering functions for temperatures between 1000 and 700 K. The present results for the $N = 5184$ atoms sample agree well with our observations for the $N = 648$ atoms sample at and below

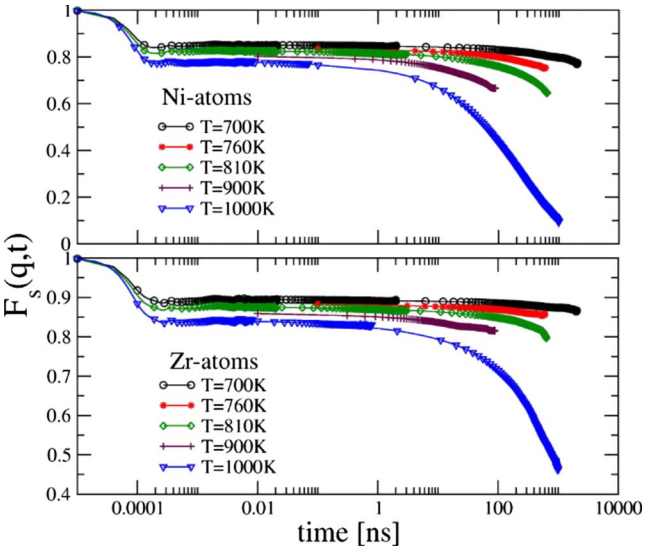

FIG. 4. (Color online) Incoherent intermediate scattering function $F_s(q,t)$ in simulated $Ni_{0.5}Zr_{0.5}$ for Ni and Zr atoms at $q = 21.6$ nm^{-1}. (Decreasing plateau values belong to increasing temperatures.)

900 K [14], and like the latter, they are in accordance with our early data [20,21]. In the correlation function, the plateau with negligible slope over three decades in time is clearly visible for temperatures below 1000 K. Its extension is smaller at 1000 K.

1. *Low-frequency* 700-K *dynamics for* $\tau = 3$ ns

Figure 5 presents the mean cluster size $\bar{S}_w(\Delta t)$ of CCMA at 700 K from LF-filtered dynamics with $\tau = 3$ ns and varying Φ values. Around $\Delta t = 16.6$ ns, the figure shows a peak in the normalized mean cluster size for Φ values between 0.07 and 0.11, which shifts to a lower Δt and reduced height for $\Phi = 0.05$ and vanishes for $\Phi = 0.03$. This behavior reflects the fact that the related CCMA are fully included in the CMA for fractions $\Phi \geqslant 0.07$. For lower Φ the mobility limit increases so much that the connectivity of the corresponding CCMA gets lost, yielding a reduced peak height at $\Phi = 0.05$ and its vanishing for $\Phi = 0.03$. Our further presentation mainly relies on $\Phi = 0.07$.

2. *Low-frequency* 700 K *dynamics for* $\Phi = 0.07$ *and varying* τ

Figure 6 provides the normalized mean size of clusters of most mobile atoms with $\Phi = 0.07$ deduced from LF 700 K dynamics in simulated $Ni_{0.5}Zr_{0.5}$ with $\tau = 0.1-4$ ns and the all-frequency case $\tau = 0$. By low-pass filtering, the maximum mean cluster size shifts from about 1.48 atoms for the unfiltered case to 12.8 for LF dynamics for $\tau \geqslant 3$ ns. At the same time, the interval Δt_{max} for the maximum of $\bar{S}_w(\Delta t)$ reduces from 160 to 16.6 ns.

A heuristic interpretation of the low-frequency dynamics can be given in terms of individual dynamical events that are localized in space and time. These events may be the avalanches or bursts of mobile atoms described in our recent analysis of irreversible, heterogeneous low-temperature dynamics [12–14]. $\Delta t_{max} = 16.6$ ns means that for this interval length optimum conditions are found between the balance of

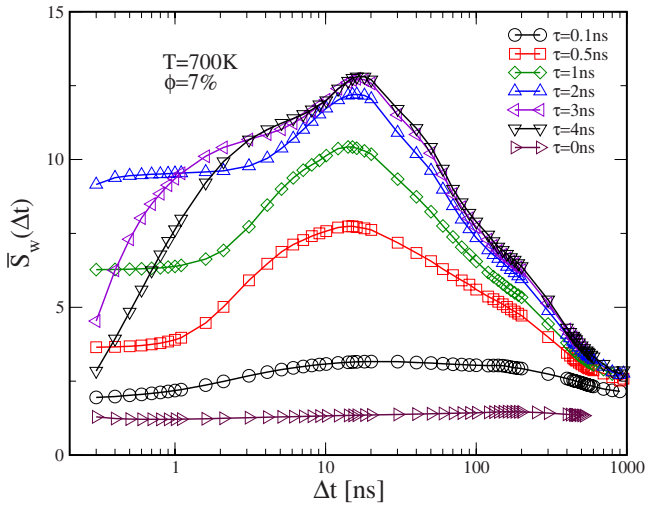

FIG. 6. (Color online) Normalized mean size of connected clusters of mobile atoms from low-frequency dynamics in simulated $Ni_{0.5}Zr_{0.5}$ as a function of interval length Δt at $T=700$ K and $\Phi=0.07$ for τ between 0.1 and 4 ns and the all-frequency case $\tau=0$.

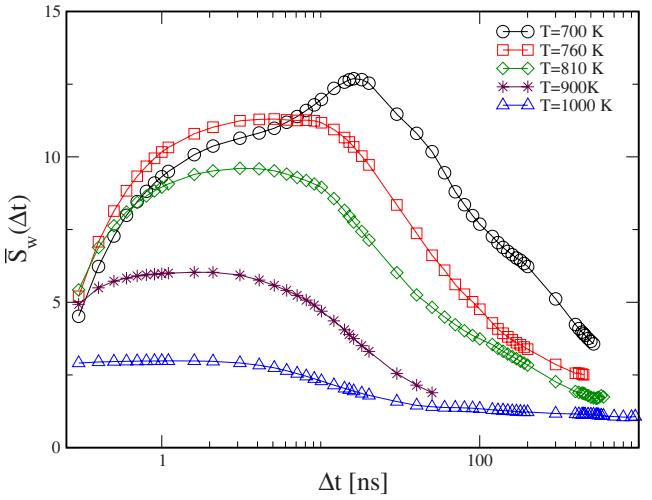

FIG. 7. (Color online) Normalized mean size of connected clusters of mobile atoms from low-frequency dynamics ($\tau=3$ ns) in simulated $Ni_{0.5}Zr_{0.5}$ as a function of interval length Δt and fraction value $\Phi=0.07$ for various temperatures between 700 and 1000 K.

having sufficient large clusters in a large fraction of the intervals, but low probability to have more than one local event in one and the same interval. In the case of fixed Φ considered here this latter situation necessarily yields a decrease of the counted cluster size.

In Fig. 6 the AF dynamics $\tau=0$ reflects disperse small-cluster events. The figure indicates that they are not counted in the LF CCMA, a behavior expected for reversible, short-time fluctuations. The amplitudes of these fluctuations determine the apparent mobility ascribed to the involved atoms. Apparently, for a significant number of these reversible short-time fluctuations the amplitudes are large enough to spoil in the AF dynamics the effects of the LF clusters. The value $\Delta t_{max}=160$ ns, found for the AF dynamics, means that for this interval length accumulation of the mobility from reversible fluctuations provides clusters of mobile atoms with maximum size on average.

3. Temperature dependence of the size of mobile clusters in low-frequency dynamics

In Fig. 7 we display the normalized mean cluster size $\bar{S}_w(\Delta t)$ from LF dynamics with $\tau=3$ ns and $\Phi=0.07$ for temperatures between 700 and 1000 K. The 700-K curve exhibits the peak already described above. At higher temperatures there are apparently competing clusters which hinder the formation of large CCMA at the given Φ.

Figure 8 presents the maximum of the normalized mean size of mobile clusters in LF dynamics, $\bar{S}_{max}(T,\tau)$, and the related interval length Δt_{max} as a function of temperature. In detail, Fig. 8(a) displays the interval length Δt_{max} from AF dynamics and from LF dynamics with $\tau=3$ μs and $\Phi=0.07$. It demonstrates that Δt_{max} from LF dynamics is significantly below the AF values for T between 700 and 900 K.

Figure 8(b) shows $\bar{S}_{max}(T,\tau)$ at $T=700$, 900, and 1000 K for $\tau=0.5$, 1.0, 2.0, and 3.0 ns and, in addition, the AF data. The figure reveals a marked τ dependence of $\bar{S}_{max}(T,\tau)$. To take care of this, we introduce an optimum value $\bar{S}^{opt}_{max}(T)$, defined by the maximum $\bar{S}_{max}(T,\tau)$ for varying τ at fixed T. Without a detailed analysis one sees from Fig. 8(b) that $\bar{S}^{opt}_{max}(T)$ is close to $\bar{S}_{max}(T,\tau=3$ ns) in the range between 700 and 900 K, while there are clear deviations at higher temperatures. For example, around 1000 K the maximum of $\bar{S}_{max}(T,\tau)$ is found below $\tau=1$ ns. For a quantitative analysis, we have designed an interpolation scheme in the T-τ plane for $\bar{S}_{max}(T,\tau)$ sketched in the Appendix. Values of $\bar{S}^{opt}_{max}(T)$ estimated from this scheme are included in Fig. 8(b) as the thick line. These data confirm the preceding conclusion about the relationship between $\bar{S}^{opt}_{max}(T)$ and $\bar{S}_{max}(T,\tau)$, and they demonstrate that $\bar{S}^{opt}_{max}(T)$ tends to approach continuously the AF value $\bar{S}_{max}(T,\tau=0)$ with increasing temperature.

From Fig. 8(b) (and Fig. 12 in the Appendix), one sees that $\bar{S}_{max}(T,\tau)$ at 900 K as a function of τ has its maximum at a value τ_{opt} between 1 and 2 ns. The decrease of $\bar{S}_{max}(T,\tau)$ for τ values above and below τ_{opt} gives additional information on the processes governing $\bar{S}_{max}(T,\tau)$. A decrease of $\bar{S}_{max}(T,\tau)$ with decreasing τ obviously means that large CCMA are split into shorter ones when τ is reduced. This can be explained in the way that atoms from large CCMA are squeezed out from the total CMA by atoms from separate, additional reversible excitations with large atomic mobility and short lifetime. The latter average out at larger τ and are of effect only at lower τ. A decrease of $\bar{S}_{max}(T,\tau)$ with increasing τ reflects a different process. There is a simple explanation for such a behavior if the large value of $\bar{S}^{opt}_{max}(T)$ is due to a low density of large CCMA having a large frequency in time. In this case, an increase of the averaging time τ leads to an apparent larger density of CCMA in each time interval. At fixed Φ, the competition between the increased numbers of CCMA necessarily yields a lower value $\bar{S}_{max}(T,\tau)$ with increasing τ and vice versa.

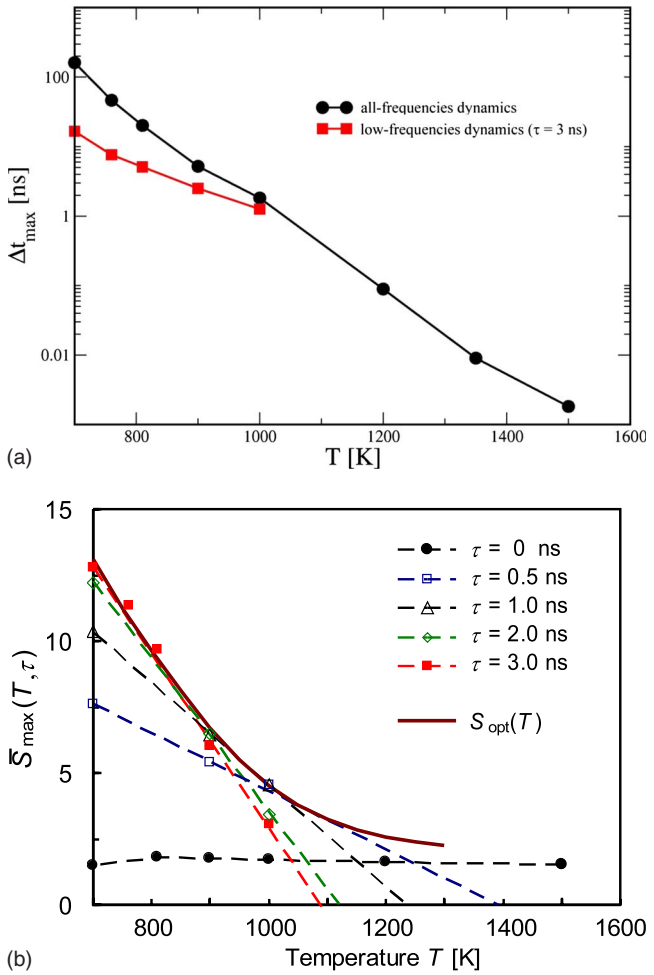

FIG. 8. (Color online) Maximum value $\bar{S}_{\max}$ of the normalized mean size of connected clusters of mobile atoms and interval length $\Delta t_{\max}$ of the maximum in simulated $Ni_{0.5}Zr_{0.5}$ as a function of temperature. (a) $\Delta t_{\max}$ from all-frequency and low-frequency (τ =3 ns) dynamics. (b) $\bar{S}_{\max}(T,\tau)$ from all-frequency (τ=0) and low-frequency (τ=0.5, 1.0, 2.0, 3.0 ns) dynamics (symbols) as well as $\bar{S}^{\text{opt}}_{\max}(T)$ (thick line). (The dashed lines are guides to the eye, only.)

From competition of both types of processes at a given T, the maximum value of $\bar{S}_{\max}(T,\tau)$ results. This provides the T dependence of $\bar{S}^{\text{opt}}_{\max}(T)$ and yields the decrease of $\bar{S}^{\text{opt}}_{\max}(T)$ with increasing T. The competition between both types of processes makes it such that $\tau_{\text{opt}}(T)$ varies by a factor of about 5 between 700 and 1000 K (compare Fig. 12), while under the same temperature change the onset of α decay in Ni-ISF shifts by a factor of 300 (compare Fig. 4). Between 1000 and 700 K, a similar shift by a factor of 200–300 is seen in the simulated Ni-diffusion coefficient [31,32] and is expected for the crossover time between the plateaulike cage regime and the onset of diffusion according to the simulated mean-square displacements of Ni atoms [14].

Figure 9 demonstrates the effects of low-pass filtering on the cluster size distribution. It presents $P(n,\Delta t_{\max})$, the probability of finding connected clusters of n atoms in the system when analyzing the most mobile atoms in the time interval $\Delta t_{\max}$ at which the maximum cluster size is found. Included

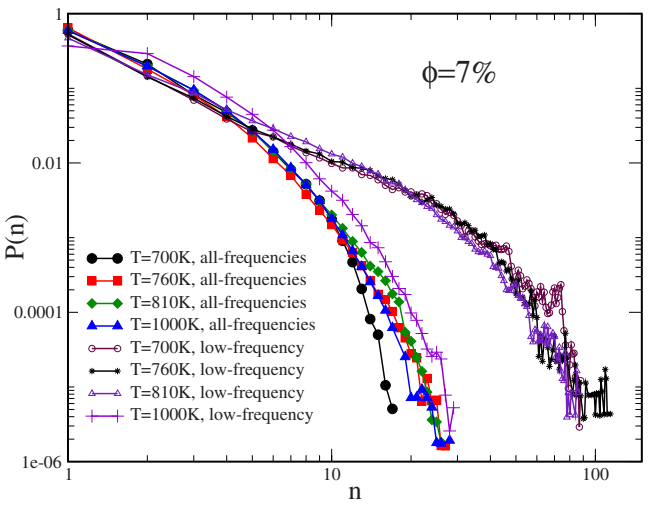

FIG. 9. (Color online) Log-log plot of the probability distribution $P(n,\Delta t_{\max})$ of the size of connected clusters from low-frequency (τ=3 ns) and all-frequency dynamics in simulated $Ni_{0.5}Zr_{0.5}$ for interval lengths $\Delta t_{\max}$ at different temperatures.

are the data for the AF and for τ=3 ns LF dynamics at 700, 760, 810, and 1000 K by taking a mobile fraction Φ=0.07. We limit ourselves to τ=3 ns regarding the fact that the corresponding $\bar{S}_{\max}(T,\tau)$ is close to $\bar{S}^{\text{opt}}_{\max}(T)$ in the relevant temperature range between 700 and 900 K.

Figure 9 indicates that in LF dynamics the probability for large clusters is increased compared to the AF case and that there is a marked probability to find significantly larger clusters in the LF case than in the AF situation. Up to two pronounced deviations, the temperature dependence of $P(n,\Delta t_{\max})$ is small when considering separately LF and AF data. However, for larger n, the AF 700-K distribution is markedly below the further AF curves, and the LF 1000-K distribution is in the range of the AF values, well below the other LF data. The behavior of the LF 1000-K distribution reflects the fact that LF $\bar{S}_{\max}(T,\tau$=3 ns) is close to AF $\bar{S}_{\max}(T,\tau$=0) for this temperature. The deviation of the AF 700-K distribution indicates the decrease of the AF mean cluster size at this temperature.

IV. DISCUSSION

Making use of a cluster size analysis (e.g., [7–10]), we investigated for simulated vitrifying $Ni_{0.5}Zr_{0.5}$ melt the size of cooperatively rearranging atom clusters that provide the probing of configuration space during the evolution of the system. In particular, for temperatures around and below 1000 K, we compare the clusters characterizing low-frequency dynamics (below the GHz scale) with those from all-frequency dynamics. For the considered temperatures the former clusters describe the processes that take place in the range of α decay, while the latter include, in addition, the reversible vibrations of the system, with frequencies typically above the 10-GHz limit.

As already discussed, Fig. 8 demonstrates that below 1000 K the maximum mean size of CCMA in LF dynamics,

expressed by $\bar{S}_{\max}^{\mathrm{opt}}(T)$, is markedly above the values from AF dynamics, which means a significant difference in the correlations of LF and AF processes.

Regarding this, one has to remember that a clear separation of the time scales of high-frequency and low-frequency dynamics is no longer possible at temperatures above 1000 K. This can be invoked from the missing of the flat plateau in the intermediate scattering functions in this temperature range [20,21]. Accordingly, well above 1000 K there is no natural separation of time scales between short-time vibrations and the long-time processes of α decay. The processes continuously merge in the way described by the mode-coupling theory when taking into account the effects of transversal currents [29,30] around and below T_c.

A. All-frequency dynamics

In Sec. III A we already addressed the agreement between the increase of maximum cluster size from AF dynamics observed here with decreasing temperature down to 810 K and the earlier CCAM data [7–10,23–26]. There is, however, a marked deviation between the earlier data and the present ones regarding the absolute value of the maximal normalized cluster size. Our maximal $\bar{S}_w$ values vary from 1.53 to 1.83 for temperatures between 1500 and 810 K, and thus are much smaller than found for other systems.

Clearly, the small maximum values are due to specific features of the present system. In order to elucidate the underlying details, we shall recall that the large clusters of mobile atoms from LF dynamics are not visible in AF dynamics. According to this, as sketched in Sec. III B 2, the displacements taken into account in LF dynamics are smaller than those visible in the mobile clusters of AF dynamics. On the other hand, the processes dominating AF dynamics are not visible in the LF dynamics. This means that the AF clusters involve reversible, high-frequency excitations, either atom vibrations or reversible over-barrier excitations (chains) of atoms with relatively large amplitudes, but short lifetimes.

Closer analysis of the clusters with maximum size at 810 K reveals that the set of most mobile clusters contains 86% Ni and 14% Zr atoms, only. As already mentioned in Sec. II C 2, it is a particular feature of the present system that Ni-Ni nearest-neighbor pairs are energetically unfavorable and occur with reduced probability, as visible in the RDF, Fig. 2. Hence, the Ni subsystem is a fragile structure with much fewer nearest-neighbor bridges than expected in a random dense distribution of spheres. Consequently, in a CMA consisting mainly of Ni atoms, we shall find only small CCMA, since connecting bridges are rare. In such a set, the size of connected clusters will markedly increase by immersing Zr atoms acting as additional multiple bridging centers. According to this, the low fraction of Zr atoms in the set of most mobile atoms explains the low size of connected clusters in this set.

Support to this arguing is given by the $S_{\max}$ value from AF dynamics at 700 K. Here a value of 1.42 follows from Fig. 3, in comparison to 1.83 for 810 K. By inspection of the CMA from AF dynamics at 700 K with $\Delta t = \Delta t_{\max}$, we find, indeed, a reduction of the Zr content to 9.5% at 700 K.

The strong decrease of the Zr content from 810 to 700 K means that at this temperature a further, Ni-rich dynamical process takes over, which provides atomic displacements larger than those of mixed Ni-Zr excitations active around 810 K. It is tempting to assume that these processes are in-cage vibrations of Ni atoms in special environments with large amplitudes. They clearly will have excitation energies lower than most of the over-barrier motions, which makes that with decreasing temperature the thermal weight shifts toward the in-cage vibrations.

This explanation implies that at 700 K, below the Kauzmann temperature T_K, individual atomic in-cage vibrations, commonly considered as the dominating dynamic processes in a solid, significantly determine the CMA on account of chainlike excitations, which are the dynamic processes typical for a liquid around T_c.

B. Clusters of most mobile atoms from low-frequency dynamics

At 700 K, our analysis of LF dynamics yields for the maximal size of most mobile clusters $\bar{S}_{\max} = 12.7$ [compare Fig. 8(b)]. This value is nearly one order of magnitude larger than the maximal cluster size from AF dynamics. Also, in this case, an explanation of the comparably large cluster size can be given in terms of the chemical composition of the sets of most mobile atoms: Closer inspection shows that for LF dynamics at 700 K and time intervals $\Delta t_{\max} = 16.6$ ns, the set of most mobile atoms consists on average of 60% Ni and 40% Zr atoms. Obviously, the Zr atoms again play the role of multiple bridging nodes and thus markedly increase the probability of finding large clusters of connected atoms. Regarding the probability of cluster sizes, Fig. 9 indicates that for 700–810 K the probability for large clusters with $n > 10$ increases in the case of LF dynamics by one or more orders of magnitude compared to the AF data.

For LF dynamics with $\tau = 3$ ns, the interval length of maximal $\bar{S}_w$, $\Delta t_{\max}$, is found between 1 and 16.6 ns at 1000–700 K. It is within the late β regime of mode-coupling theory [11] for this system. Compared to the AF value, the LF $\Delta t_{\max}$ is reduced, e.g., at 700 K, by one order of magnitude. The shift of $\Delta t_{\max}$ makes that at 700 K the ratio between the crossover time t^*, which means the onset of α decay, and the $\Delta t_{\max}$ value for LF dynamics becomes $t^*/\Delta t_{\max} \approx 35$.

This value clearly is outside the estimates from the AF results and from the previous CSA studies around T_c [7–10]. As we already mentioned in Sec. II B, a heuristic interpretation of the $\Delta t_{\max}$ value from LF dynamics at 700 K can be given in terms of avalanches or bursts of dynamical active groups of atoms localized in space and time. In this case, the interval length with maximum mean cluster size is not directly related to the diffusion decay of structure. It follows from different demands: (i) There is the demand to increase Δt to have sufficient large time intervals to pick up a maximum number of atoms associated with a burst. (ii) There is the demand to reduce the interval length in order to reduce the probability for having more than one local event in one and the same interval. At fixed Φ, the occurrence of two

locally separated events with strong displacements will reduce the apparent maximal size of connected clusters in most cases.

In this picture, interpretation of the ratio $t^*/\Delta t_{\max}$ needs understanding of the interrelationship between the set of mobile atoms and the overall diffusion of atoms, since the crossover time t^* signals a beginning of the dominance of diffusion against in-cage motion. Regarding this interrelationship we can conclude from the present data that it needs about 35 times $\Delta t_{\max}$ to fill space sufficiently dense with local dynamic events to provide an appreciable contribution to the irreversible diffusion of particles. For completeness, we here shall recall that the Ni diffusion coefficient of our system in the glassy state between 700 and 1050 K is in reasonable agreement with experiments for glassy $Ni_{0.5}Zr_{0.5}$ [31,32]. (For Zr in amorphous $Ni_{0.5}Zr_{0.5}$, to our best knowledge, self-diffusion data are not available in the literature.) In the case of Ni, our model yields an Arrhenius-type behavior with activation energy $Q=1.2$ eV and a pre-exponential factor $D_0=5\times10^{-7}$ m^2/s, while the experiments give $Q=1.3$ eV and $D_0=1.7\times10^{-7}$ m^2/s [33]. Hence, the LF dynamics analyzed here and the related sets of most mobile atoms provide the magnitude of irreversible particle dynamics expected from experiments.

According to the above given explanation, $\Delta t_{\max}$ from LF dynamics characterizes the time after which the atoms begin to lose the character pertaining to the set of most mobile ones. Regarding this, Fig. 10(a) displays for $\Phi=7\%$ and $\tau=3$ ns the set of most mobile atoms at 700 K with $t\in[t_1,t_1+\Delta t_{\max}]$, $t_1=32.5$ ns. For the present system of 5184 atoms in the periodicity box, the figure displays that the CMA is localized in space and fills only a limited part of the system, which mans that the CCMA have a tendency to form higher-level clusters in space. Figure 10(b) depicts the CMA in the later time interval $[t_2,t_2+\Delta t_{\max}]$, $t_2=150$ ns, for otherwise the same conditions as Fig. 10(a). Comparison of the two figures makes obvious that the CMA, which means the region of LF dynamic activity, has changed its shape and shifts within about 120 ns from the left-hand side of the periodicity box to its middle. The shift takes place by shrinking of the set of most mobile atoms in some regions of space and growing in other ones. This means calming down of the relative LF dynamics of atoms in the former regions compared to the latter, where the latter grow by initiation of sufficiently large irreversible or long-lasting displacements of atoms adjacent to the CMA.

More information about the spatial propagation of LF CMA is given by Fig. 11. The figure displays the LF mobility autocorrelation function $K(t)$, which measures the probability that a particle belonging to the LF CMA at time t_1 is found in the LF CMA at the later time t_1+t, too. In detail, $K(t)$ is defined as

$$K(t)=N_c^{-1}\left\langle\sum_n p_n(t_1+t)p_n(t_1)\right\rangle, \tag{6}$$

with $p_n(t)=1$ if $n\in X(t,\Delta t,\Phi,\tau)$, and $p_n(t)=0$ otherwise. In Eq. (6) the brackets denote averaging over time t_1. Figure 11 shows $K(t)$ for the parameters $T=700$ K, $\Phi=0.07$, $\tau=3$ ns, and $\Delta t=16.6$ ns.

In the figure, there are two regimes visible, a short-time one up to some 20 ns, where $K(t)$ decays rather rapidly from 1 to about 0.4, and a long-time tail reaching far beyond the analyzed limit of 300 ns. The short-time decay reflects rapid correlated transitions of a larger number of atoms, like the previously analyzed bursts or avalanches. Due to averaging with $\tau=3$ ns, the mobility parameter from irreversible (or LF) events will be smeared out over about 6 ns even when the events take place on a scale well below 3 ns. Regarding this, Fig. 11 implies that about half of the atoms in an LF CMA participate only in short-time events like the avalanches.

The long-time tail reflects slow propagation of the CMA in space, as visible when comparing Figs. 10(a) and 10(b), which demonstrate the spatial changes within 117.5 ns. Although Fig. 11 does not allow a proper estimate of the long-tail decay time, it is obvious that the time scale for this decay is the μs regime. It is this time scale that characterizes LF CMA propagation at 700 K.

Now comes the question whether there is sufficient independence of the CMA from the particular prescription used to identify such a set. Regarding this, we found that an alternative definition of atomic mobility by the quantity [15]

$$\delta w_j^2(t)=\int_{-\infty}^{\infty}dt'[\vec{r}_j(t)-\vec{r}_j(t')]^2\exp[-(t-t')^2/2\tau^2]/\sqrt{2\pi\tau^2} \tag{7}$$

yields a comparable CMA as Eq. (2), provided the same values are used for the fraction Φ and the smoothing time τ. For demonstration, Fig. 10(c) presents the CMA for the same conditions as Fig. 10(a), but relying on the mobility definition, Eq. (7), instead of Eq. (2). There is fair agreement between these two sets concerning their extension in space, although not all atoms from the latter are found in the former.

Closer analysis shows for the special example of Fig. 10(c) that 73% of the atoms pertaining to the set from mobility definition, Eq. (2), also are found in the LF set based on the mobility measure, Eq. (7). This value is close to the average over 600 intervals $[t,t+\Delta t_{\max}]$ with varying t, giving a mean correlation of $72\%\pm6\%$ from comparing both sets for each interval. According to our analysis [14,16], the CMA have to be visualized as arrangements with high mobility in the interior and continuous decrease of mobility in the outer regions. The deviations between the two sets from different measures of mobility reflect, in this context, that the ranking of atoms according to mobility varies to a certain extent with the measure used. This necessarily makes it such that different atoms are selected as members of the CMA due to the sharp limit set by a fixed fraction value Φ.

As we already addressed in a recent paper [15], it is tempting to correlate the local LF dynamics events with the objects of "defect models" that currently have gained increasing interest (e.g., [3–6]) as tools to approach the thermodynamics of the glass transition. Promoting the concept of dynamic facilitation (DF), Garrahan and Chandler [3,4] consider in a coarse-grained picture volume elements in a "mobile" state, which are the centers of LF dynamics in the vit-

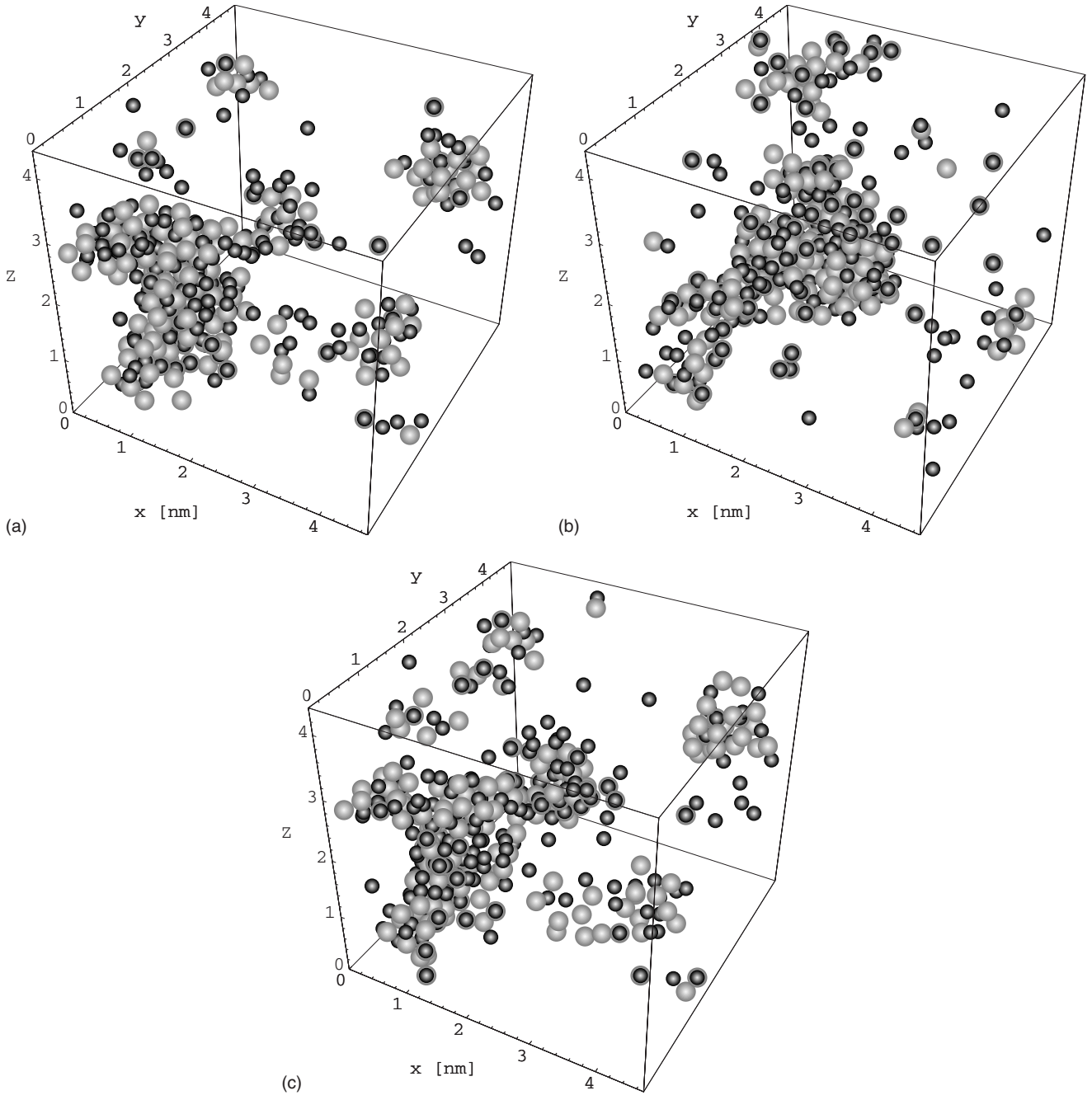

FIG. 10. Cluster of most mobile atoms in simulated $Ni_{0.5}Zr_{0.5}$ at 700 K for $\Phi=0.07$, $\tau=3$ ns, and time interval $[t_0, t_0+\Delta t_{max}]$. (a) Mobility according to Eq. (2) and time interval beginning at $t_0=32.5$ ns, (b) mobility according to Eq. (2) and time interval beginning at $t_0=150$ ns, and (c) mobility according to Eq. (7) and time interval beginning at $t_0=32.5$ ns.

rifying melt, while the environmental material undergoes only reversible high-frequency fluctuations that are responsible for the major part of the thermal excitation energy in the sample. In the DF picture, volume elements in the mobile state form excitation lines in the space-time continuum, which in space coalesce, branch, and percolate with time [3,4]. There are indications that in this picture α decay takes place on the time scale within which a sufficient fraction of total space has turned into the mobile state and is sufficiently rearranged at least once [34]. Our observation concerning the time evolution of the sets of most mobile atoms and their propagation in space in essence agrees with this assumption. These features, which we also detected in our previous studies [12–15] on LF dynamics in NiZr glass, substantiate our finding that exploration of the PEL and metabasin transitions takes place by processes on the low-frequency scale, either by chain-type excitation within a CMA or by bursts or avalanches [12,14], where processes of the latter type now have attracted much interest under the keyword *democratic particle motion* [17,34–36].

The LF CMA have also features ascribed to the mobile zones by Matyushov and Angel in their theory of the glass transition [6]. Due to the local dynamics, the LF CMA efficiently scan large regions of phase space and hence carry

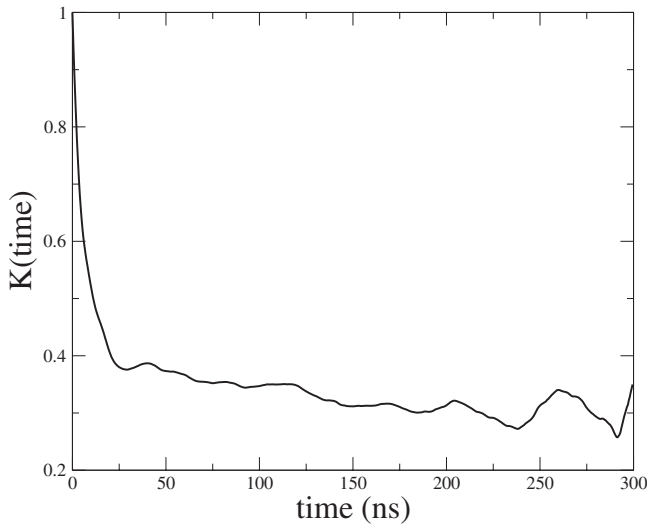

FIG. 11. LF mobility autocorrelation function $K(t)$, measuring the probability that a particle belonging to the LF CMA at time t_1 is also found in the LF CMA at the later time t_1+t, for $T=700$ K, $\Phi=0.07$, $\tau=3$ ns, and $\Delta t=\Delta t_{\max}$.

important parts of the configuration entropy of the vitrifying melt, which is an essential feature of the mobile zones in the treatment of Matyushov and Angel.

The present results are in accordance also with the recent concept of dynamic propensities of Widmer-Cooper *et al.* [37,38]. As discussed in [15], in the present $Ni_{0.5}Zr_{0.5}$ system there is a marked correlation between the regions of LF dynamics, which means the CMA, and structural inhomogeneity. For the analyzed temperature regime between 700 and 810 K, a significant correlation exists between local LF dynamics and averaged cage volume around Ni atoms or (a combination of) the Q_n parameter of Steinhardt *et al.* [39], with correlation values from 0.75 to 0.8 [15]. Moreover, the correlation value between the local LF dynamics and the potential energy of the atoms increases from 0.05 at 700 K to 0.33 at 810 K [15], supporting the assumption for a correlation between these quantities at higher temperatures, in agreement with the recent analysis for a system of water molecules [40].

V. SUMMARY AND CONCLUSIONS

From the present analysis, there emerges the following picture about the glass transition in vitrifying melts: Around the critical temperature T_c, there is the separation of time scales predicted by the mode-coupling theory and, as a consequence, a separation of high-frequency (HF) and LF dynamics. The HF dynamics describes vibrations and reversible over-barrier excursions of (groups of) atoms. The LF dynamics includes reversible low-frequency and, in particular, irreversible structural changes responsible for α decay and the viscous relaxations of the system.

The LF dynamics takes place in clusters (LF CMA) localized in space, a feature already seen in our previous studies about the LF dynamics [13–15]. Within an LF CMA, the dynamics is carried by events localized in space and time.

TABLE I. Parameters a_{kj} used in the interpolation scheme for $\bar{S}_{\max}(T,\tau)$.

$k\backslash j$	0	1	2
1	248.16	−461.17	242.67
2	−748.87	1752.30	−1091.80
3	771.10	−1920.60	1220.40

These are the bursts or avalanches of our previous studies [13–15] for the NiZr model, which recently also have been found in the Lennard-Jones system [17] and now have attracted much interest as democratic particle motion [17,34,36]. These events include groups of up to about 100 connected atoms from the LF CMA, which move in a correlated manner (compare also [16]).

The LF CMA have the features of mobile zones in the dynamical facilitation picture of Garrahan and Chandler [3,4] or the glass transition model by Matyushov and Angel [5], and they show significant correlations between local LF dynamics and structural heterogeneity [15] as considered by the concept of dynamical propensity by Widmer-Cooper *et al.* [37,38].

The localized LF CMA propagate in space. According to our present estimate, the LF CMA have at 700 K a decay time in the μs range, which agrees rather well with our recent estimate for the onset of α decay in the quenched system at this temperature [14]. At this temperature, the limited number of LF CMA and their slow propagation in space causes the extreme high viscosity of the vitrifying system. This makes it tempting to assume that vitrification of the melts under cooling is due to heterogeneous dynamics with decreasing density of LF CMA, the latter being characterized by a decreasing propagation velocity in space. Consequently, a crucial feature of vitrification is the slowing down of the

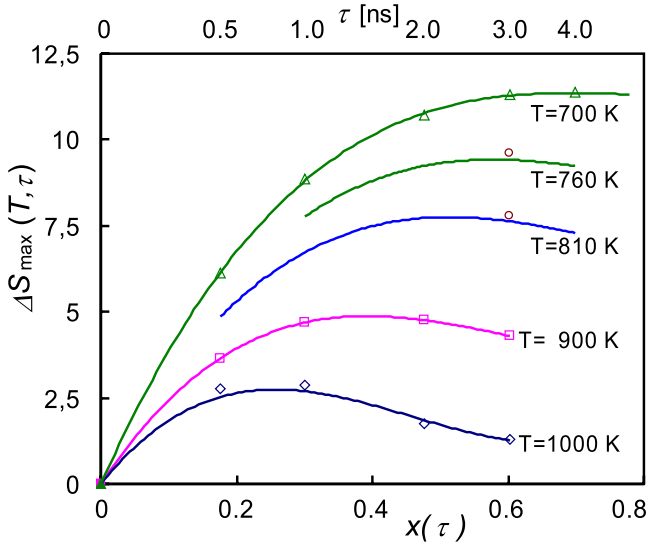

FIG. 12. (Color online) $\Delta\bar{S}_{\max}(T,\tau)$ from MD simulations for $Ni_{0.5}Zr_{0.5}$ at various T and τ (symbols) and interpolation of the data according to Eqs. (A2)–(A4) with parameters a_{kj} from Table I (lines).

propagation of the CMA in space with decreasing temperature, which implies a slowing down of the propagation of the related structural inhomogeneity.

ACKNOWLEDGMENT

The authors gratefully acknowledge support by the ZAM Jülich by providing computer capacity on the JUMP system for carrying out the calculations.

APPENDIX

For interpolating the simulated $\bar{S}_{\max}(T,\tau)$ data of Fig. 8(b) we use the scheme

$$\bar{S}_{\max}(T,\tau) = \bar{S}_{\max}(T,\tau=0) + \Delta\bar{S}_{\max}(T,\tau), \tag{A1}$$

$$\Delta\bar{S}_{\max}(T,\tau) = \sum_{k=1}^{3} a_k(T)x(\tau)^k, \tag{A2}$$

$$x(\tau) = \log_{10}(1+\tau/[\mathrm{ns}]), \tag{A3}$$

$$a_k(T) = \sum_{j=0}^{2} a_{kj}(T/1000\ \mathrm{K})^j, \tag{A4}$$

with parameters a_{kj} from Table I. Figure 12 shows $\Delta\bar{S}_{\max}(T,\tau)$ from our simulation at 700, 900, and 1000 K together with the interpolation curves according to Eq. (A2) as a function of $x(\tau)$. $\bar{S}^{\mathrm{opt}}_{\max}(T)$ in Fig. 8(b) is deduced from the maximum of $\Delta\bar{S}_{\max}(T,\tau)$, Eq. (A2), at fixed T.

[1] G. Adam and J. H. Gibbs, J. Chem. Phys. **43**, 139 (1965).
[2] W. Kauzmann, Chem. Rev. (Washington, D.C.) **43**, 219 (1948).
[3] J. P. Garrahan and D. Chandler, Phys. Rev. Lett. **89**, 035704 (2002).
[4] D. Chandler and J. D. Garrahan, J. Chem. Phys. **123**, 044511 (2005).
[5] D. V. Matyushov and C. A. Angell, J. Chem. Phys. **123**, 034506 (2005).
[6] J. S. Langer, Phys. Rev. E **73**, 041504 (2006).
[7] C. Donati, S. C. Glotzer, P. H. Poole, W. Kob, and S. J. Plimpton, Phys. Rev. E **60**, 3107 (1999).
[8] S. C. Glotzer, J. Non-Cryst. Solids **274**, 342 (2000).
[9] Y. Gebremichael, M. Vogel, and S. C. Glotzer, J. Chem. Phys. **120**, 4415 (2004).
[10] M. Vogel and S. C. Glotzer, Phys. Rev. E **70**, 061504 (2004).
[11] W. Götze and L. Sjögren, Rep. Prog. Phys. **55**, 241 (1992).
[12] H. Teichler, J. Non-Cryst. Solids **293-295**, 339 (2001).
[13] H. Teichler, J. Non-Cryst. Solids **312-314**, 533 (2002).
[14] H. Teichler, Phys. Rev. E **71**, 031505 (2005).
[15] I. Ladadwa and H. Teichler, Phys. Rev. E **73**, 031501 (2006).
[16] K. Vollmayr-Lee, W. Kob, K. Binder, and A. Zippelius, J. Chem. Phys. **116**, 5158 (2002); K. Vollmayr-Lee and A. Zippelius, Phys. Rev. E **72**, 041507 (2005).
[17] G. A. Appignanesi, J. A. Rodríguez Fris, R. A. Montani, and W. Kob, Phys. Rev. Lett. **96**, 057801 (2006).
[18] C. Hausleitner and J. Hafner, Phys. Rev. B **45**, 115 (1992).
[19] M. W. Finnis, J. Phys. F: Met. Phys. **4**, 1654 (1974).
[20] H. Teichler, Phys. Rev. Lett. **76**, 62 (1996).
[21] H. Teichler, Phys. Rev. E **53**, R4287 (1996).
[22] H. Teichler, Phys. Rev. B **59**, 8473 (1999).
[23] Y. Gebremichael, T. B. Schröder, F. W. Starr, and S. C. Glotzer, Phys. Rev. E **64**, 051503 (2001).
[24] M. Aichele, Y. Gebremichael, F. W. Starr, J. Baschnagel, and S. C. Glotzer, J. Chem. Phys. **119**, 5290 (2003).
[25] M. N. J. Bergroth, M. Vogel, and S. C. Glotzer, J. Phys. Chem. B **109**, 6748 (2005).
[26] M. V. Y. Gebremichael and S. C. Glotzer, Mol. Simul. **30**, 281 (2005).
[27] M. Guerdane and H. Teichler, Phys. Rev. B **65**, 014203 (2001).
[28] K. Suzuki, T. Fukunaga, K. Shibata, T. Otomo, and M. Mizuseki, in *Thermodynamics of Alloy Formation*, edited by Y. A. Chang and F. Sommer (Minerals, Metals, and Materials Society, Warrendale, PA, 1997), p. 125.
[29] S. P. Das and G. F. Mazenko, Phys. Rev. A **34**, 2265 (1986);
[30] W. Götze and L. Sjögren, J. Phys. C **21**, 3407 (1988); L. Sjögren, Z. Phys. B: Condens. Matter **79**, 5 (1990).
[31] H. Teichler, Defect Diffus. Forum **143-147**, 717 (1997).
[32] F. Faupel, W. Frank, M.-P. Macht, H. Mehrer, V. Naundorf, K. Rätzke, H. R. Schober, S. K. Sharma, and H. Teichler, Rev. Mod. Phys. **75**, 237 (2003).
[33] R. S. Averback, Mater. Res. Bull. **16**, 47 (1991).
[34] L. O. Hedges and J. P. Garahan, e-print arXiv:0706.0902
[35] A. C. Pan, J. P. Garrahan, and D. Chandler, Phys. Rev. E **72**, 041106 (2005).
[36] M. Elenius and M. Dzugutov, e-print arXiv:0711.1061v1.
[37] A. Widmer-Cooper, P. Harrowell, and H. Fynewever, Phys. Rev. Lett. **93**, 135701 (2004).
[38] A. Widmer-Cooper and P. Harrowell, Phys. Rev. Lett. **96**, 185701 (2006).
[39] P. J. Steinhardt, D. R. Nelson, and M. Ronchetti, Phys. Rev. B **28**, 784 (1983).
[40] G. S. Matharoo, M. S. Gulam Razul, and P. H. Poole, Phys. Rev. E **74**, 050502(R) (2006).